Or-348

ANL-76-58 ANL-76-58

206
9-14-76
UC-79b Plus UK + Germany

A UNIFIED AND MECHANISTIC APPROACH TO CREEP-FATIGUE DAMAGE

by

S. Majumdar and P. S. Maiya

APPLIED TECHNOLOGY

Any further distribution by any holder of this document or of the data therein to third parties representing foreign interests, foreign governments, foreign companies and foreign subsidiaries or foreign divisions of U. S. companies should be coordinated with the Director, Division of Reactor Development and Demonstration, U. S. Energy Research and Development Administration.

MASTER

The facilities of Argonne National Laboratory are owned by the United States Government. Under the terms of a contract (W-31-109-Eng-38) between the U. S. Energy Research and Development Administration, Argonne Universities Association and The University of Chicago, the University employs the staff and operates the Laboratory in accordance with policies and programs formulated, approved and reviewed by the Association.

MEMBERS OF ARGONNE UNIVERSITIES ASSOCIATION

The University of Arizona
Carnegie-Mellon University
Case Western Reserve University
The University of Chicago
University of Cincinnati
Illinois Institute of Technology
University of Illinois
Indiana University
Iowa State University
The University of Iowa
Kansas State University
The University of Kansas
Loyola University
Marquette University
Michigan State University
The University of Michigan
University of Minnesota
University of Missouri
Northwestern University
University of Notre Dame
The Ohio State University
Ohio University
The Pennsylvania State University
Purdue University
Saint Louis University
Southern Illinois University
The University of Texas at Austin
Washington University
Wayne State University
The University of Wisconsin

NOTICE

[illegible] of work sponsored [illegible] the United States [illegible] and Development Administration [illegible] any of their [illegible] makes any [illegible] any legal liability [illegible] accuracy, completeness or usefulness [illegible] product or process [illegible] would not infringe [illegible] of commercial products, [illegible] in this publication [illegible] approval or disapproval of the [illegible] Laboratory or the U. S. Energy [illegible]

Distribution Category:
LMFBR Fuels and Materials
Engineering and Development
(UC-79b)

ANL-76-58

ARGONNE NATIONAL LABORATORY
9700 South Cass Avenue
Argonne, Illinois 60439

A UNIFIED AND MECHANISTIC APPROACH TO CREEP-FATIGUE DAMAGE

by

S. Majumdar and P. S. Maiya

Materials Science Division

January 1976

TABLE OF CONTENTS

LIST OF FIGURES

LIST OF FIGURES (Contd.)

LIST OF TABLES

NOMENCLATURE

English Letters

A, T, C, m, k	Cyclic material parameters
A', T'	Monotonic values of A [illegible]
A_{eff}	Effective value of A [illegible]
a_o, a, a_c	Initial, current, and [illegible]
D_T, D_C, D	Damage during tensile [illegible], respectively
N, N_f	Cycles and cycles to [illegible]
N_{cp}	Partitioned fatigue life
N_{f_o}	Cycles to failure at [illegible]
t, t_f	Time and time to failure, [illegible]
t_H	Hold time

Greek Letters

α	Constant
$\Delta\epsilon_{cp}$	Partitioned strain range
$\Delta\epsilon_p$, $\Delta\epsilon_t$	Plastic and total strain [illegible], respectively
$\Delta\sigma_{relax}$	Total stress relaxation during [illegible]
ϵ_f	Ductility defined as [illegible] in cross-sectional area at rupture
ϵ_p, ϵ_t	Plastic and total strain, respectively
$\epsilon_{p_{max}}$, $\epsilon_{p_{min}}$	Plastic strain at beginning of tensile and [illegible] time, respectively
$\dot{\epsilon}_m$	Rising mean strain rate
$\dot{\epsilon}_p$, $\dot{\epsilon}_t$, $\dot{\epsilon}_{p_{ave}}$	Plastic, total, and average plastic strain rate, respectively
ν	Frequency of cycling
σ	Current stress
σ_{max}	Maximum stress during cycling
σ_o, σ_o', t_o, t_1, B, B'	Parameters to describe stress relaxation
τ	Time period = $1/\nu$, where ν is frequency
τ_o, τ_1	Constants

A UNIFIED AND MECHANISTIC APPROACH TO CREEP-FATIGUE DAMAGE

by

S. Majumdar and P. S. Maiya

ABSTRACT

A new creep-fatigue damage-rate equation is proposed that takes into account both plastic strain and strain rate. The coefficients and exponents in the damage-rate equation are interpreted by means of the various damage mechanisms of the material. The damage-rate equation has been integrated to analyze various phenomena such as the effects of plastic strain rate on monotonic tensile or creep rupture time, rising mean strain on the low-cycle fatigue behavior at elevated temperature, tensile and compressive hold times on the low-cycle fatigue life at elevated temperature, and cyclic creep. The proposed approach has been successfully applied to elevated-temperature data generated at Argonne National Laboratory and elsewhere for Type 304 austenitic stainless steel under various monotonic and cyclic-loading conditions.

The approach does not separate the inelastic strain into plastic (time independent) and creep (time dependent) components. The method recognizes that the effect of plastic strain rate on the damage process is of major importance and takes into account the fact that the damage encountered in any deformation path depends not only on the plastic strain accumulated but also on the rate at which the plastic strain is accumulated. Thus, the damage due to several loading histories of interest can be computed in a simple and unified manner.

I. INTRODUCTION

Low-cycle fatigue at elevated temperature is an important consideration in the design and operation of structural components for many nuclear and non-nuclear applications. Fatigue failure can occur under the combined action of creep and fatigue, which involves a complex strain-cycling pattern. This situation makes creep-fatigue interaction sensitive to variables such as temperature, wave-shape pattern, strain rate, and environment. Despite the active interest and the work concerning this problem, creep-fatigue interaction remains a challenging area of research and is perhaps one of the most poorly understood phenomena both from a fundamental and technological viewpoint.

Argonne National Laboratory (ANL) has been involved in the generation and analysis of high-temperature, low-cycle creep-fatigue data for Types 304 and 316 austenitic stainless steel. The present study suggests that the currently recommended methods of evaluating creep-fatigue interaction in ASME code case 1592[1] should be improved.

Historically, most of the approaches developed to include the interaction between low-cycle fatigue and creep have been an extension of the low-temperature description of low-cycle fatigue behavior, e.g., Manson's Universal slopes and 10% rule[2] and Coffin's frequency-modified fatigue life equations.[3,4] The method of Universal slopes and 10% rule does not recognize the effects of strain rate and hold times. Coffin has demonstrated that frequency is important in high-temperature, low-cycle fatigue. The frequency effect is identical to the strain-rate effect only for the case of continuous cycling. However, for tests involving hold times at constant total strain, the stress relaxes and the plastic strain rate decreases continuously during the hold time. The detrimental effect of tensile hold times on fatigue lives is now fairly well established[5-7] for most materials. This is not surprising because a lowering of the strain rate is associated with more and more grain-boundary sliding (and other effects that may result from an active environment), and, consequently, more damage to the material occurs resulting in intergranular failure. The frequency-modified method fails to take into account the deformation and fracture processes when cycles with various wave shapes are applied. [Recently, Coffin (private communication) proposed a frequency-separation method to take into account wave-shape effects.] The recognition of the fact that creep and plastic deformation affect the damage processes differently has led to the development of the strain-range-partitioning technique.[8,9] Although this approach considers the effects of wave shapes, the rate at which the creep or plastic strain is accumulated is ignored. For example, in the partitioning of the total plastic strain range into $\Delta\varepsilon_{cp}$ (tensile creep reversed by compressive plastic flow), it is assumed that the damage due to cyclic creep and cyclic relaxation are identical. However, data generated for Type 304 stainless steel have shown[10] that the "cp" strain accumulated in cyclic relaxation is more damaging than in cyclic creep, a result which can only be rationalized in terms of strain-rate effects. Another approach for creep-fatigue interaction often discussed is the linear life fraction damage rule proposed by Robinson[11] and Taira, as discussed by Spera.[12] This method has not been successful because of the inherent assumption that the damage process occurs (in a material under a creep-fatigue situation) linearly with time and cycle. In addition, all the existing methods are not readily amenable to the incorporation of the effects associated with more complicated wave shapes other than the ones used by the investigators in their experimental program. For example, no method exists that can predict the effect of rising mean strain in low-cycle fatigue at elevated temperatures.

The above discussion is not intended as a criticism of the existing approaches but rather is an attempt to appreciate the merits of and accept the limitations inherent to the predictive tools. Furthermore, the deficiencies cannot be removed by additional refinements. It should be pointed out that the predictive methods proposed and discussed by Coffin and Manson have led other investigators to seek new data and search for new alternative approaches which will lead to a better understanding of creep-fatigue interaction.

The present work recognizes the fundamental importance of plastic strain rate in the damage process. When postulating a single damage-rate equation in terms of plastic strain and strain rate (which may be justified from a mechanistic viewpoint), the various processes associated with the effects of strain rate on the time to rupture during creep or monotonic tensile loading, or the effects of strain rate, hold times, and rising mean strain on fatigue lives, can be quantitatively analyzed in a simple and unified manner. To date, the method has been applied successfully to data generated for Type 304 stainless steel at 1100°F (593°C) under a variety of loading conditions. It is also worth mentioning that both Coffin's frequency-modified equation and Manson's partitioned strain-range equations can be derived by applying the proposed damage equation to specific loading conditions.

II. BASIC DAMAGE EQUATION

We assume that a characteristic microcrack length a is a measure of the accumulated damage and the failure of a low-cycle fatigue specimen occurs as a re[illegible] the extension of such preexisting microcracks or flaws of initial le[illegible] to a critical length of a_c, at which point one or more microcracks li[illegible]rm a macrocrack. The macrocrack, once formed, propagates rapidly through the specimen. The time spent in the propagation of a macrocrack is, in general, small compared with the total time in a typical low-cycle fatigue test.[13] In practice, a_0 might correspond to, for example, the inherent defect size or the size of surface irregularity of the specimen, and a_c might correspond to a few grain diameters. But, as will be seen, exact values of these parameters are not required as long as specimens with identical geometry and microstructure are used. Furthermore, we assume that the growth of each microcrack is governed by the following equation.

$$\frac{da}{dt} = \begin{cases} aT\,|\epsilon_p|^m\,|\dot{\epsilon}_p|^k & \text{(In the presence of tensile stress)} \\ aC\,|\epsilon_p|^m\,|\dot{\epsilon}_p|^k & \text{(In the presence of compressive stress)} \end{cases} \tag{1}$$

where a, ϵ_p, and $\dot{\epsilon}_p$ are the current microcrack length, plastic strain, and plastic strain rate, respectively, and t is time. T, C, m, and k are material parameters that are functions of temperature, environment, and metallurgical condition of the material but are constants over limited ranges of plastic strains and strain rates. Although stress does not appear explicitly in Eq. (1), it is implicitly involved, because the plastic strain and the plastic strain rate can be related to the stress by an equation-of-state theory similar to that proposed by Hart.[14] Ideally, a material structure state variable instead of plastic strain should be used in Eq. (1). For the loading cases considered in the present report, the plastic strain reflects the material structure state variable.

For continuous cycling over a plastic strain range $\Delta\epsilon_p$ at a constant plastic strain rate $\dot{\epsilon}_p$, Eq. (1) can be integrated (Appendix A) to give the cycles to failure as

$$\int_{a_0}^{a_c} \frac{da}{a} = N_f \left[2(T + C) \int_0^{\tau/4} |\dot{\epsilon}_p t|^m \; |\dot{\epsilon}_p|^k \, dt \right] .$$

where $\tau = \frac{2\Delta\varepsilon_p}{\dot{\varepsilon}_p}$.

Performing the above integration and solving for N_f,

$$N_f = \frac{m+1}{4A}\left(\frac{\Delta\varepsilon_p}{2}\right)^{-(m+1)} (\dot{\varepsilon}_p)^{1-k} , \quad (2)$$

where

$$A = \frac{C+T}{2} \Bigg/ \ln\frac{a_c}{a_o} . \quad (2a)$$

For tests that involve specimens with identical geometry and microstructure, A can be considered as a material parameter. Equation (2) can be expressed in terms of the frequency of cycling (ν) instead of the plastic strain rate as

$$N_f = \frac{m+1}{4A}\left(\frac{\Delta\varepsilon_p}{2}\right)^{-(m+k)} (4\nu)^{1-k} . \quad (3)$$

Equation (3) is identical to the frequency-modified life equation proposed by Coffin.[3]

As mentioned earlier, ANL has been conducting an extensive series of low-cycle fatigue tests at elevated temperature for Type 304 stainless steel at a variety of total strain rates ranging from 4×10^{-6} s^{-1} to 4×10^{-2} s^{-1}. Prior to fatigue testing, all specimens were solution annealed at 1092°C for 30 min and aged at 593°C for 1000 h to achieve a fairly stable microstructure. The material parameters A, m, and k for this particular steel at 593°C were obtained by a least-squares fit of Eq. (2) to the generated fatigue life by using data of at least two strain-rate levels. The plastic strain range and strain-rate values for each test were obtained at half the fatigue life ($N_f/2$). It was found that parameters A, m, and k are not constants over the entire spectrum of strain rates. A plot of these constants versus strain rates is shown in Fig. 1. Note that parameters A and m show an abrupt transition in the strain-rate interval of 10^{-4} to 10^{-2} s^{-1}. Below a strain rate of 10^{-5} s^{-1} they appear to attain constant values. Although m approaches a constant value above a strain rate of 10^{-2} s^{-1}, sufficient high strain-rate data are not available to establish the upper plateau value of A. The parameter k, on the other hand, shows a gradual increase as the strain rates increase over the entire strain-rate spectrum of the tests. However, k should saturate at a value of unity for a high strain rate beyond which the fatigue life becomes independent of frequency or strain rate. Correlation of data for creep rupture and low-cycle fatigue life involving hold times with predicted values (discussed in Secs. III and IV) suggests that parameter k should not decrease indefinitely as the strain rate decreases. For the purpose of the present discussion, k has been assumed to saturate to a constant value of 0.525. The exact variation of k in the low strain-rate regime is unavailable because of

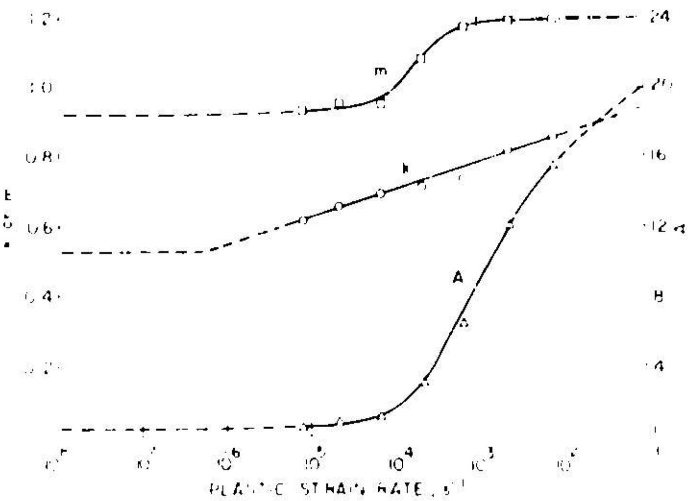

Fig. 1. Variation of Parameters A, m, and k with Plastic Strain Rate for Type 304 Stainless Steel at 593°C. Neg. No. MSD-61799.

the lack of continuous-cycling fatigue data in this region. A good estimate for the lower saturation value of k can be obtained from the monotonic creep-rupture data (Sec. IV). Thus, parameters A, k, and m display an S-shape transition behavior. This transitional behavior can be associated with a change in the fracture mechanism observed in the low-cycle fatigue testing of the material from a predominantly transgranular mode (with striations on the fractured surface) to a predominantly intergranular mode (no striations, Fig. 2).

It should be emphasized that, for predictive purposes over a limited range of strain rates, A, k, and m can be treated as constants. For example, over the range of strain rates from 10^{-4} s^{-1} to 4×10^{-2} s^{-1}, the use of average values of A = 11.84, k = 0.81, and m = 1.19 gives reasonable prediction of fatigue life, as shown in Fig. 3. Similarly, values of A = 0.45, k = 0.62, and m = 0.93 give reasonable predictions for tests carried out at strain rates ranging from 4×10^{-6} s^{-1} to 4×10^{-5} s^{-1}, as shown in Fig. 4.

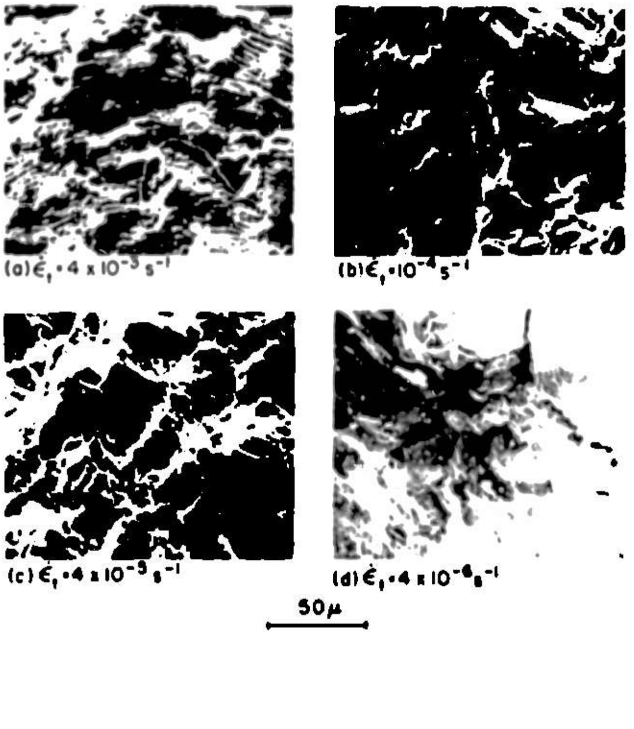

Fig. 2. Series of Scanning-electron Micrographs Showing Effects of Strain Rate on Appearance of Fatigue Fracture Surface. Neg. No. ANL-306-75-230.

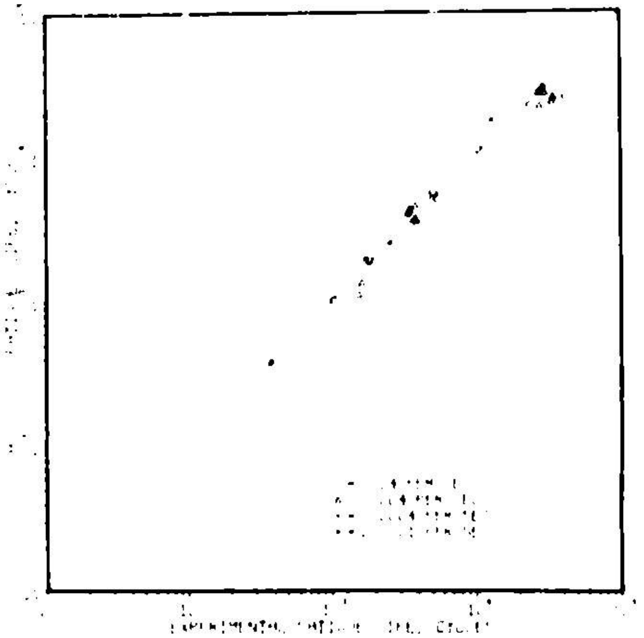

Fig. 3. Comparison of Experimentally Observed Low-cycle Fatigue Lives of Type 304 Stainless Steel at 593°C during Continuous Cycling with Calculated Values using Average Material Parameters A = 11.84, k = 0.81, and m = 1.19. Neg. No. MSD-61792.

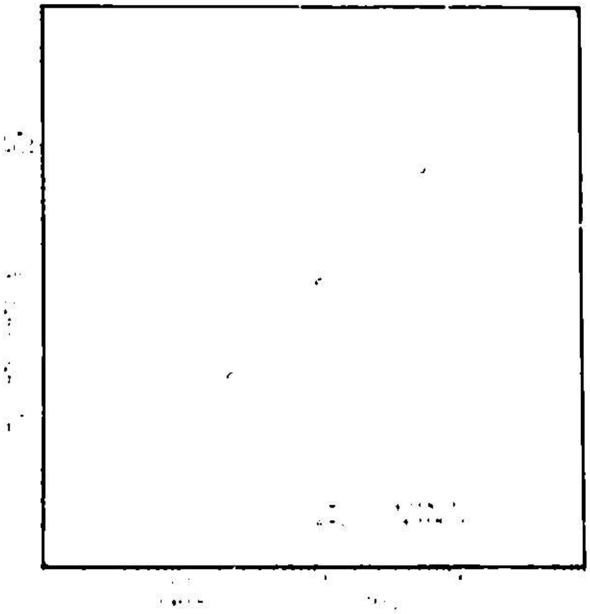

Fig. 4. Comparison of Experimentally Observed Low-cycle Fatigue Lives of Type 304 Stainless Steel at 593°C during Continuous Cycling with Calculated Values using Average Material Parameters A = 0.45, k = 0.62, and m = 0.93. Neg. No. MSD-61793.

Although these tests were performed at constant total strain rate rather than at constant plastic strain rate, the error in assuming a constant plastic strain rate can be shown to be small, as discussed in Appendix B.

III. HOLD-TIME EFFECTS IN LOW-CYCLE FATIGUE

Consider a fatigue test in which a predetermined period of hold time at constant total strain is imposed both at the maximum tensile strain and the maximum compressive strain limits in addition to cycling at a given strain range with zero mean strain. When the hold times in tension and compression are equal, the tests will be referred to as tests with symmetric hold times. On the other hand, fatigue tests can be run where only tensile hold time is applied with zero compressive hold time or vice versa. These three types of tests that involve hold-time periods ranging from 1 min/cycle to 600 min/cycle have been carried out at ANL for Type 304 stainless steel at 593°C. In the majority of these tests, the stress relaxes rapidly at the beginning of the hold time, and the relaxation data show an instantaneous drop in stress because the recording instrument does not have adequate response time. Part of the drop in stress is due to anelastic effects and should be nondamaging. In any case, the rapid drop in stress implies a high plastic strain rate over a short period of time and consequently causes little damage. Beyond the initial drop in stress, the stress-relaxation behavior can be described by the following equation:

$$\sigma = \sigma_0 - B \ln t, \qquad \text{for } t > t_1, \tag{4}$$

where σ_0, B, and t_1 are constants for a particular test. It should be noted that Garofalo[15] and Conway et al.[16] have also observed similar stress-relaxation behavior for many materials including Type 304 stainless steel. For shorter times during the hold-time period, Eq. (4) has been extrapolated by means of the following equation:

$$\sigma = \sigma_0' - B' \ln (t + t_0), \qquad \text{for } t < t_1, \tag{5}$$

such that the initial condition of stress is satisfied. However, the damage in the short and intermediate time periods in all cases is found to be small compared with the damage accumulated at large t where Eq. (4) is valid.

When computing the damage during a hold-time fatigue experiment, we note that the plastic strain rate is constant and the plastic strain changes during the cyclic part of the loading, whereas the plastic strain is approximately constant and the plastic strain rate varies during the hold-time periods. Thus, integrating Eq. (1) with respect to time and crack length,

$$\int_{a_0}^{a_c} \frac{da}{a} = N_f \left[2(T + C) \int_0^{\tau/4} |\dot{\epsilon}_p t|^m \, |\dot{\epsilon}_p|^k \, dt + |\epsilon_{p_{max}}|^m \right.$$

$$\left. \int_0^{t_H} T \, |\dot{\epsilon}_p|^k \, dt + |\epsilon_{p_{min}}|^m \int_0^{t_H} C \, |\dot{\epsilon}_p|^k \, dt \right].$$

Using Eq. (2a) the above equation can be reduced to

$$\frac{1}{N_f} = \frac{4A}{m + 1} \left(\frac{\Delta\epsilon_p}{2}\right)^{m+1} (\dot{\epsilon}_p)^{k-1} + |\epsilon_{p_{max}}|^m \int_0^{t_H} \frac{2A}{1 + C/T} \, |\dot{\epsilon}_p|^k \, dt$$

$$+ |\epsilon_{p_{min}}|^m \int_0^{t_H} \frac{2A}{1 + T/C} \, |\dot{\epsilon}_p|^k \, dt, \tag{6}$$

where $\epsilon_{p_{max}}$ is the plastic strain at the beginning of the tensile hold time, $\epsilon_{p_{min}}$ is the plastic strain at the beginning of compressive hold time, and t_H is hold time. We define the first term on the right-hand side of Eq. (6) as the cyclic damage per cycle and the second and third terms as the hold-time damage per cycle. It should be mentioned that the above approach does not imply that the damage per cycle, i.e., the crack-growth per cycle, is constant throughout life. Also, it should be noted that the cyclic damage is computed using the appropriate values for parameters A, k, and m, depending on the plastic strain rate during cycling. The hold-time damage, on the other hand, is calculated by numerical integration using the appropriate values of the parameters that correspond to the plastic strain rate, which varies continuously during the hold time.

Table I shows a representative sample of hold-time fatigue data together with the lives that have been computed using Eq. (4) and the various stress-relaxation data at half life from each of these tests, as shown in Figs. 5-11. The maximum stress at which relaxation begins, the total stress relaxation, and the plastic strain rates at the midpoint and end of the hold-time period are also reported in Table I. The plastic strain rates are obtained by fitting the stress-relaxation data to Eqs. (4) and (5) and then differentiating and dividing by Young's modulus, taken to be 150 × 10^3 MPa.[17] When computing the damage during hold time, the value of T is assumed to be four times greater than the value of C. This assumption seems to predict the compressive and symmetric hold-time data reasonably well. However, it should be pointed out that fatigue data with compressive hold times are not extensive, and the compressive hold times used are not of sufficient length to firmly establish that T = 4C. Note that compressive relaxation behavior is quite similar to the tensile relaxation behavior for the test with symmetric hold time (Fig. 10). However, the stress-relaxation curve for the test with symmetric hold time is significantly different from that of the test with tensile hold only. The less detrimental effect of symmetric hold time compared with tensile hold time can thus be explained for Type 304 stainless steel in terms of the different stress-relaxation behavior. The last two tests in Table I refer to cyclic creep tests in tension hold only, i.e., the tensile stress was held constant during the hold-time period of each cycle, and the specimen was allowed to creep until a predetermined amount of total strain was reached. Because the maximum stress during hold time could not be controlled exactly at the same value in each cycle, the creep rate and, consequently, the hold-time period varied significantly from cycle to cycle. The creep rates and hold times used for calculating fatigue life were obtained by averaging over ten cycles at approximately the half life of each test. Note that in all cases the predicted life differs by less than a factor of two from the experimentally observed life.

IV. TENSILE AND CREEP RUPTURE

During a monotonic tensile or creep test, we assume a crack-growth (or void-growth) law similar to Eq. (1) as follows:

$$da/dt = a\,T'\,|\epsilon_p|^m\,|\dot{\epsilon}_p|^k\,, \tag{7}$$

where T', in general, is different than T, but k and m are identical with those used in Eq. (1). [Correlation of measured time to tensile and creep-rupture data with predicted values for Type 304 stainless steel at 593°C suggests that parameters k and m which determine the slope of the plot of rupture time versus strain rate, Eq. (8), are the same under both monotonic and cyclic loading conditions for this particular material.] With the assumption that $\dot{\epsilon}_p$ is the constant total strain rate during a tensile test and is the steady-state creep rate during a creep test, integration of Eq. (7) leads to

TABLE 1. Comparison of Predicted Values with Experimentally Observed Low-cycle Fatigue Lives of Type 304 Stainless Steel at 593°C and Various Hold Times

Test No.	$\Delta\epsilon_t$, %	$\Delta\epsilon_p$, %	$\dot{\epsilon}_t$	t_H,[a] min	σ_{max},[a] MPa	σ_{relax}, MPa	$\dot{\epsilon}_p$ AT ($t = t_H/2$ s^{-1})	$\dot{\epsilon}_p$ AT ($t = t_H$ s^{-1})	Average Damage/Cycle: Hold Time	Average Damage/Cycle: Cyclic	Predicted N_f	Experimental N_f
617	2.005	1.6996	4×10^{-3}	60T	269.6	86.9	6.33×10^{-6}	3.17×10^{-6}	0.00639	0.00456	91	102
661	0.996	0.7247	4×10^{-3}	60T	230.3	46.0	2.93×10^{-6}	1.46×10^{-6}	0.00200	0.00113	320	305
543	2.068	1.677	4×10^{-3}	1T	306.7	57.2	2.37×10^{-6}	1.19×10^{-6}	0.000442	0.00183	440	378
612	2.004	1.659	4×10^{-3}	15T	304.0	79.3	1.65×10^{-7}	8.25×10^{-8}	0.00258	0.00178	229	237
663	1.984	1.662	4×10^{-3}	60T	281.1	75.8	4.34×10^{-8}	2.17×10^{-8}	0.00532	0.00179	141	112
510	2.024	1.744	4×10^{-3}	180T	288.2	104.8	2.22×10^{-8}	1.11×10^{-8}	0.0114	0.00197	75	63
135	0.9973	0.6980	4×10^{-3}	1T	228.2	45.5	9.35×10^{-7}	4.67×10^{-7}	0.000176	0.000276	2211	1664
767	1.0134	0.7577	4×10^{-3}	2S	262.0T	38.6	1.36×10^{-6}	6.79×10^{-7}	0.000152	0.000327	1908	2177
					266.8C	37.9	1.38×10^{-6}	6.92×10^{-7}	0.000045			
773	1.0212	0.7089	4×10^{-3}	4C	269.6	37.2	3.32×10^{-7}	1.66×10^{-7}	0.000105	0.000286	2554	2453
767	1.0	0.7219	4×10^{-3}	10T	228.2	37.9	1.44×10^{-7}	7.19×10^{-8}	0.000744	0.000295	962	706
618	1.004	0.744	4×10^{-3}	15T	218.5	39.3	6.39×10^{-8}	3.19×10^{-8}	0.000776	0.000314	917	666
520	1.036	0.856	4×10^{-3}	600T	188.2	60.7	6.3×10^{-9}	3.15×10^{-9}	0.00570	0.000418	165	212
154	0.5026	0.2844	4×10^{-3}	10T	162.7	12.4	1.4×10^{-7}	7.0×10^{-8}	0.000275	0.000041	3168	3803
616	0.5952	0.372	4×10^{-3}	15T	167.5	29.0	4×10^{-8}	2×10^{-8}	0.000325	0.000071	2526	2765
580	1.9879	1.6134	4×10^{-3}	48T[b]	284.8	-	3.34×10^{-7}	3.34×10^{-7}	0.0089	0.0018	93	73
553	0.982	0.6821	4×10^{-3}	6T[b]	227.5	-	2.29×10^{-7}	2.29×10^{-7}	0.00045	0.000325	1294	685

[a] T = tensile hold, C = compressive hold, and S = symmetric hold.

[b] Average hold time in cyclic creep tests.

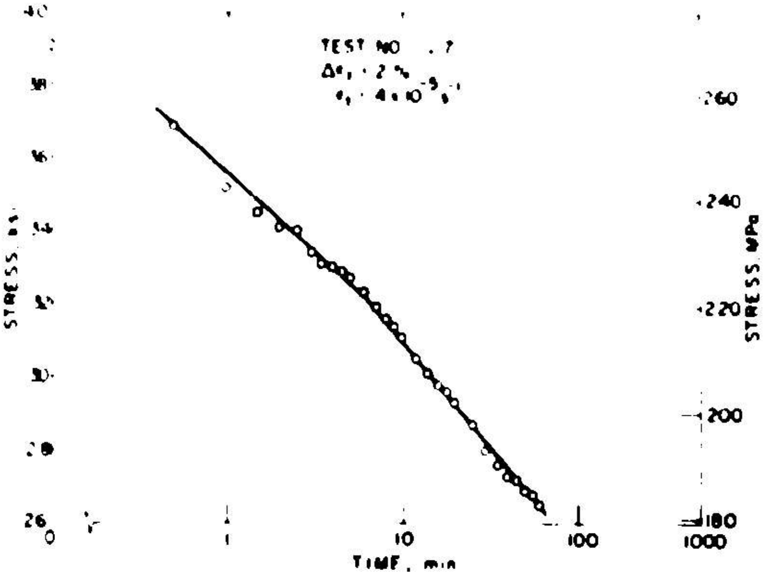

Fig. 5. Cyclic Stress Relaxation of Type 304 Stainless Steel at 593°C for a Tensile Hold Time of 60 min/cycle at 2% Strain Range. Neg. No. MSD-61802.

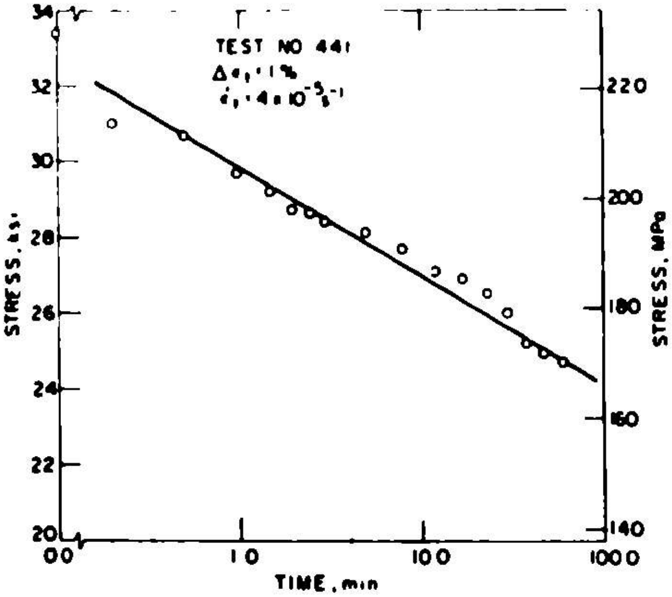

Fig. 6. Cyclic Stress Relaxation of Type 304 Stainless Steel at 593°C for a Tensile Hold Time of 60 min/cycle at 1% Strain Range. Neg. No. MSD-61803.

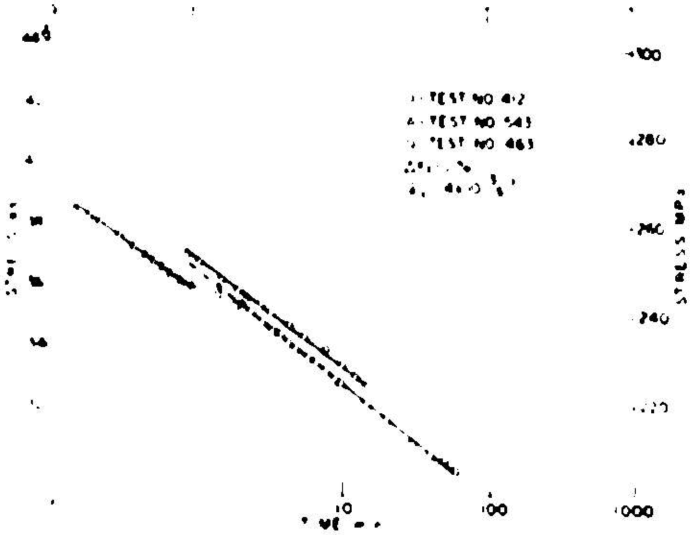

Fig. 7. Cyclic Stress Relaxation of Type 304 Stainless Steel at 593°C for Tensile Hold Times of 1, 15, and 60 min/cycle. Neg. No. MSD-61794.

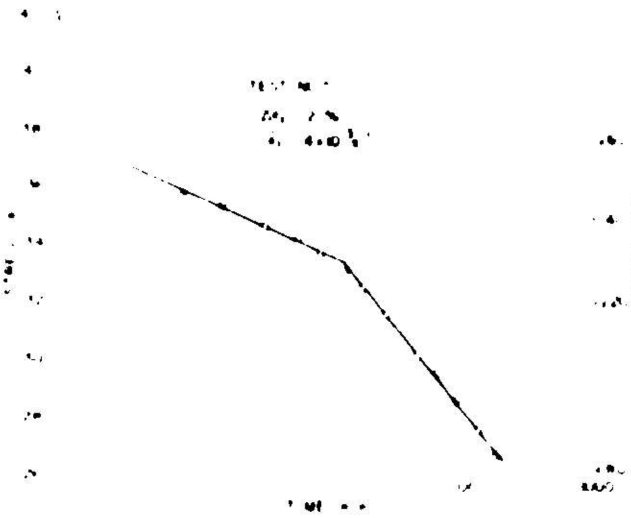

Fig. 8. Cyclic Stress Relaxation of Type 304 Stainless Steel at 593°C for a Tensile Hold Time of 180 min/cycle. Neg. No. MSD-61798.

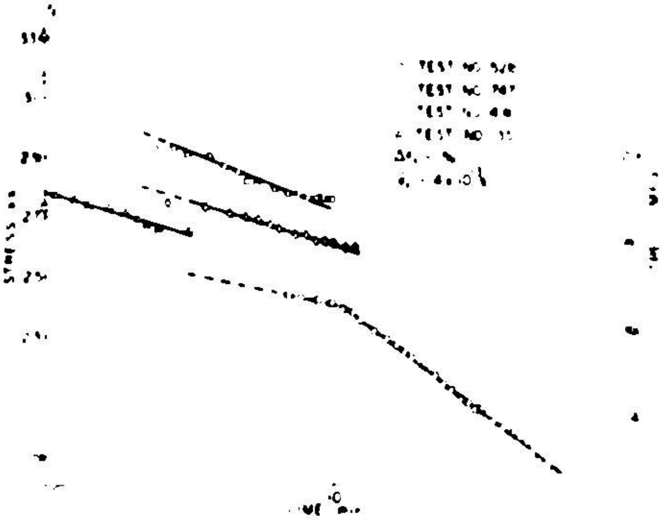

Fig. 9. Cyclic Stress Relaxation of Type 304 Stainless Steel at 593°C for Tensile Hold Times of 1, 10, 15, and 600 min/cycle. Neg. No. MSD-61796.

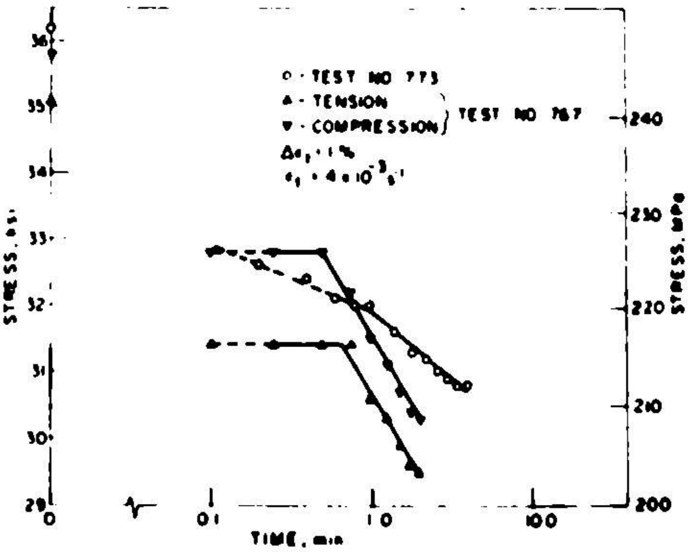

Fig. 10. Cyclic Stress Relaxation of Type 304 Stainless Steel at 593°C for a Symmetric Hold Time of 2 min/cycle and a Compressive Hold Time of 4 min/cycle. Neg. No. MSD-61800.

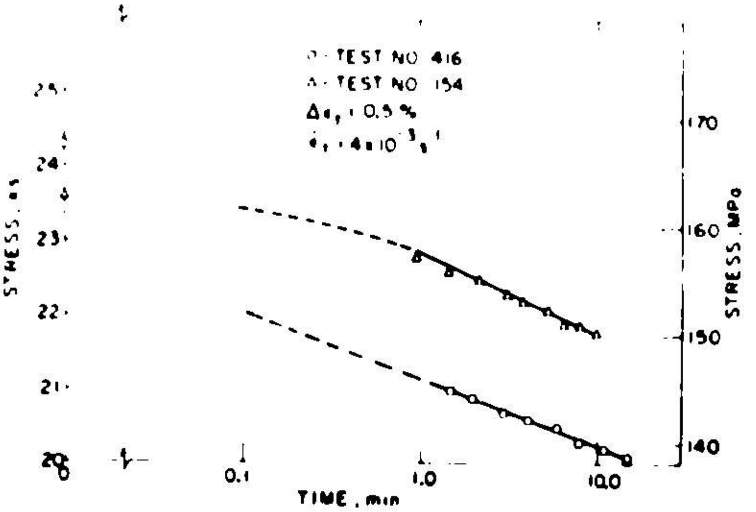

Fig. 11. Cyclic Stress Relaxation of Type 304 Stainless Steel at 593°C for Tensile Hold Times of 10 and 15 min/cycle. Neg. No. MSD-61801.

$$\int_{a_o}^{a_c} \frac{da}{a} = T' \; |\dot{\epsilon}_p|^k \int_o^{t_f} |\dot{\epsilon}_p t|^m \, dt$$

or

$$(\dot{\epsilon}_p)^{k+m/1+m} \; t_f = \left(\frac{m + 1}{T'} \; \ln \frac{a_c}{a_o}\right)^{1/m+1} = \text{constant}, \tag{8}$$

and defining $\epsilon_f = \dot{\epsilon}_p \; t_f$

$$\epsilon_f = \left(\frac{m + 1}{T'} \; \ln \frac{a_c}{a_o}\right)^{1/m+1} (\dot{\epsilon}_p)^{1-k/1+m} \; , \tag{9}$$

where t_f is the time to failure, and ϵ_f is approximately the ductility. Equation (8) is identical to the well-known Monkman-Grant relationship[18] between the steady-state creep rate and time to rupture in creep experiments. A plot of Eq. (8) using values of the parameter from Fig. 1 together with some tensile and creep-rupture data[17,19-22] for Type 304 stainless steel at 593°C is displayed in Fig. 12. Note that the data for the solution-annealed and aged material agree remarkably with the predicted values. However, data for the solution-annealed material fall below the predicted curve. This is to be expected because the predictions are based on material parameters that were determined for the solution-annealed and aged material. The long-time creep-rupture data for the solution-annealed material tend to approach the predicted curve, as would be expected. The sharp change in the slope of the predicted line (Fig. 12) corresponds to a transition from the intergranular to transgranular failure mode. The results demonstrate that parameters k and m derived from the low-cycle fatigue data are applicable to a monotonic loading situation. In addition, the results permit a comparison of cyclic and monotonic loading

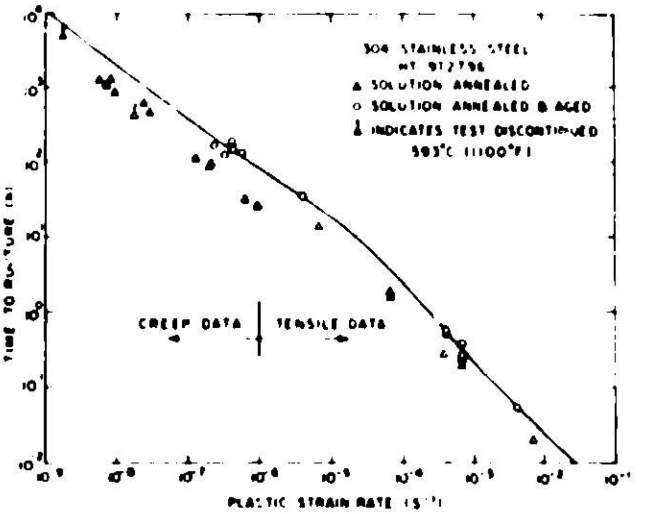

Fig. 12. Calculated and Observed Variation of Monotonic Tensile and Creep-rupture Time with Plastic Strain Rate. Neg. No. MSD-62107.

damage. For example, the value of T' required to achieve the proper level of time to rupture indicates that the damage or crack-growth rate under completely reversed cyclic loading is ~15 times higher than that under monotonic loading (i.e., $T \approx 15T'$) at the same plastic strain, strain rate, and crack length for this particular steel at 593°C.

V. EFFECTS OF RISING MEAN STRAIN ON LOW-CYCLE FATIGUE LIFE

Consider a fatigue test in which a constantly rising mean strain rate $\dot{\epsilon}_m$ is superimposed on a constant cycling at a plastic strain range of $\Delta\epsilon_p$. Integration of Eq. (1) for this particular situation leads to the following equation for cycles to failure (Appendix C):

$$N_f = \frac{1}{\alpha}\sqrt{3N_{f_o} - \frac{1}{3}} \qquad \text{for } N_f > \frac{1}{\alpha}$$

$$\alpha^2 N_f^3 + 3N_f - 3N_{f_o} = 0 \qquad \text{for } N_f < \frac{1}{\alpha}, \tag{10}$$

where

$$\alpha = \frac{4\dot{\epsilon}_m}{\dot{\epsilon}_p}, \tag{10a}$$

and

$$N_{f_o} = \frac{m+1}{4A_{eff}}\left(\frac{\Delta\epsilon_p}{2}\right)^{-(1+m)} (\dot{\epsilon}_p)^{1-k}. \tag{10b}$$

Since the mean plastic strain in a rising mean strain fatigue test increases continuously, the material never cyclically saturates completely. Consequently, the value of $A = A_{eff}$ used to compute N_{f_o} in Eq. (10b) should be approximately between the value of A for the cyclically saturated material and A', the value of A for a virgin material. Analysis of the creep-rupture data in Sec. IV showed that the cyclic parameter T was 15 times greater than the monotonic parameter T'. Since C for Type 304 stainless steel is much smaller than T, it is reasonable to assume that A, defined by Eq. (2a), $\approx$ 15A'. Since the material cyclically saturates to a greater extent under a slower rising mean strain test than under a higher rising mean strain rate test, the value of A_{eff} should be closer to A for a slower rising mean strain test than for the higher rising mean strain test.

A plot of the calculated cycles to failure, using Eqs. (10a) and (10b), versus the rising mean strain rate together with some test data for Type 304 austenitic stainless steel at 593°C are shown in Fig. 13 for two values of strain ranges. The solid lines in the figure refer to the lives corresponding to A_{eff} = A and A_{eff} = A'. However, the rising mean strain rates in all the tests are sufficiently high so that the calculated lives that correspond to A_{eff} = A' are close to the test data. Note that the lower strain range tests are more susceptible to reduction in life than the higher strain range tests carried out at the same rising mean strain rate.

Although few test data are available to bear out the predicted lives over a broad range of rising mean strain rates, the general trend in the test data is in close agreement with the predicted values.

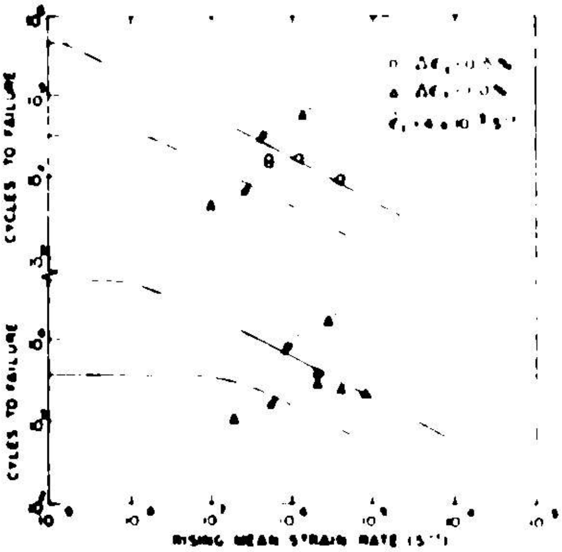

Fig. 13. Calculated and Observed Variation of Cycles to Failure of Type 304 Stainless Steel at 593°C with Rising Mean Strain Rate. Neg. No. MSD-62106.

VI. MECHANISTIC CONSIDERATIONS

The mechanistic basis for the proposed approach to damage analysis will be discussed. The approach is applicable to specimens of macroscopic size (i.e., much larger than grain size) and to cases for which severe plastic instability is absent during a major portion of the life.

We assume that three major types of damage are produced by deformation, whether monotonic or cyclic.[15,23] These are schematically represented in Fig. 14. Type A damage usually occurs at low homologous temperatures and/or at high strain rates where the deformation of the specimen is controlled by grain-matrix deformation processes. This type of damage generally leads to transgranular failure of the material. The rate of crack propagation in this type of fracture is controlled by crack geometry and applied stress.

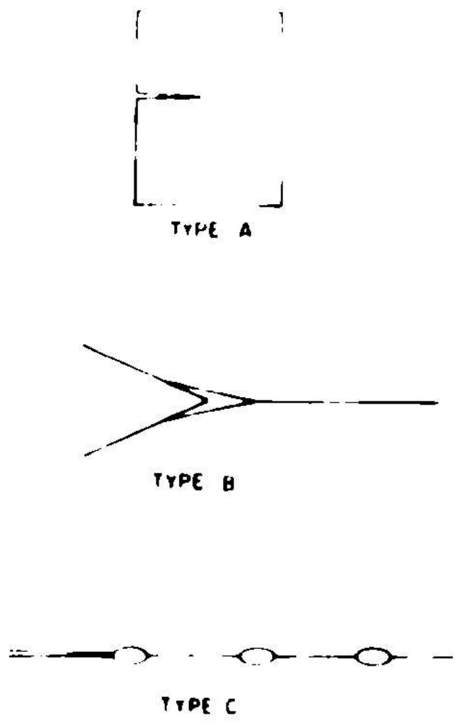

Fig. 14. Schematic Representation of Transgranular (Type A) and Intergranular (Types B and C) Damage Mechanisms during Creep-fatigue Loading Condition. Neg. No. MSD-61789.

Type B damage, in the form of wedge cracks at grain-boundary intersections, usually occurs at higher temperatures and/or lower strain rates compared with the conditions that favor type A damage. Type B damage leads to intergranular failure of the material. Grain-boundary sliding plays an important role in both the initiation and propagation of this type of crack.[15,illegible] At temperatures and strain rates where the wedge-type crack predominates, grain-boundary sliding contributes significantly to the deformation of the specimen. The incompatibility between the grain-boundary sliding and the grain-matrix deformation is the main cause of this type of crack. This type of crack can be easily initiated, particularly in the presence of cyclic loading. The extent of grain-boundary sliding also controls the rate of crack propagation. It has been shown experimentally[illegible] that, at a given temperature and strain rate, the contribution of grain-boundary sliding to plastic deformation depends upon the magnitude of the applied stress.

Type C damage, in the form of grain-boundary cavities, usually occurs at higher temperatures and/or lower strain rates than those favoring wedge-type cracks. This type of damage also leads to intergranular failure of the material. The initiation of cavities is associated with grain-boundary sliding and occurs early in life. However, its growth has been shown to be controlled by stress-induced mass transport.[illegible,25] The growth of these cavities eventually leads to link-up and results in failure. The driving force for the stress-induced mass transport is the normal stress at the grain boundary. The grain boundary serves as the source of vacancies and the cavities serve as sinks.

During the tensile hold time, the cavity growth will continue, although significant plastic deformation is absent. Since the cavity growth rate decreases as the applied tensile stress decreases, the growth rate will diminish as the stress relaxes during hold time. Under compressive stresses, cavities have been observed to shrink with time.[15] This possibility is consistent with the experimental observation that compressive hold time is less damaging than tensile hold time in many materials, and, in fact, compressive hold time would be beneficial if cavity growth by diffusion were the only damaging process.

The rate of damage due to cavity growth will depend on the cavity density. The increase in number density should result in reduced life. Evans[26] and Evans and Skelton[27] have measured the number density of grain-boundary cavities produced by both monotonic creep and cyclic deformation in a magnesium alloy. They have found that the cavity density is less by a factor of ~20 under monotonic creep than under the cyclic-loading condition. Similar observations have been made by Gittus[28] for copper. In addition, Hill[29] has noted that grain-boundary cracking in 1% Cr-Mo-V steel occurs to a greater extent in fatigue tests with hold times than in creep-rupture tests with the same time to failure.

These observations are consistent with our results, suggesting that cyclic deformation is more damaging than monotonic deformation even for the case where grain-boundary cavitation is the predominant damage mechanism.

It should be noted that, in any test, various combinations of the three types of damaging processes are possible. However, depending on the temperature and strain rate, one of the processes will be more important than the other two. The transition from one damaging process to another can be correlated with the transition in the rate-controlling processes for plastic deformation.[30,31] It is suggested that the mode of plastic deformation forms an important physical basis for the approach proposed in the present paper.

Based on the damage processes discussed previously, it is seen that the rate of damage accumulation in all cases is a function of the applied stress. According to the recent development in the plastic equation of state,[30] the magnitude of the applied stress is defined at a given temperature by the state of hardness, i.e., material structure state and plastic strain rate. Since an analytically convenient material-structure-state variable is not currently available, the plastic strain, at a given strain rate and temperature and in the absence of large thermal aging effects, is assumed to reflect the structure state of the material. Thus, together with the plastic strain rate and temperature, the plastic strain defines the applied stress.

A typical stress versus plastic strain-rate plot for a Type 316 stainless steel[32] at 500°C is shown in Fig. 15. According to the plastic equation-of-state theory,[30] the high strain-rate portion of the curve is identified as being controlled by grain-matrix deformation. As the strain rate is lowered, the contribution of grain-boundary sliding becomes important, resulting in an increase in the slope of the curve. At the low strain-rate end of the S-shape curve, the grain boundary offers little resistance to deformation such that the slope of the curve is controlled by grain-matrix deformation processes again. Similar effects of plastic strain rate on the damage processes have been discussed. The transition in the damage parameter shown in Fig. 1 occurs roughly at the same strain rates as the transition in Fig. 15. Additional development is required, however, to better understand the physical significance of the parameters used in the data analysis and also to incorporate into Eq. (1) a better measure of material-structure state than plastic strain.

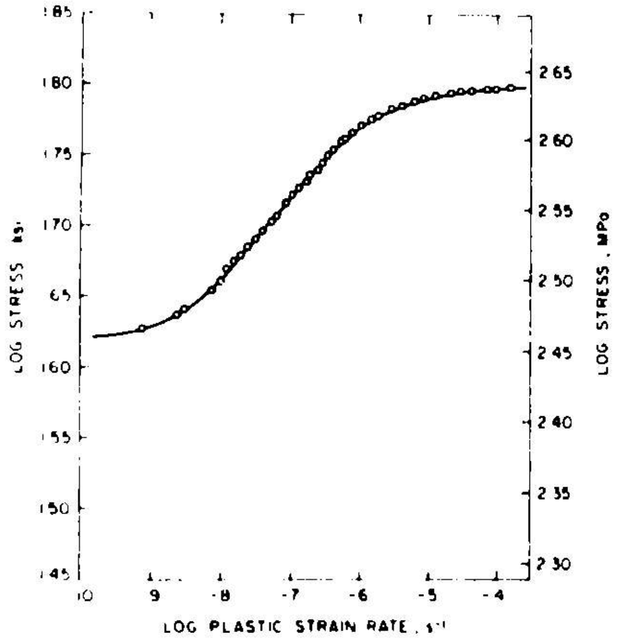

Fig. 15. Typical Stress vs Plastic Strain-rate Plot for Type 316 Stainless Steel at 600°C. Neg. No. MSD-61804.

VII. DISCUSSION OF RESULTS

In the present investigation, a creep-fatigue damage-rate equation, in terms of a current characteristic crack length, plastic strain, and plastic strain rate, has been proposed. The phenomenological theory has been used to quantitatively describe and analyze the damage phenomena encountered in monotonic creep and creep-fatigue interaction. Inherent in this approach is the recognition that the accumulated plastic strain over a deformation path as well as the rate at which the strain accumulation occurs over the path are important. The method has been used successfully to explain a representative sample of the extensive elevated-temperature data generated for austenitic Type 304 stainless steel under a variety of loading conditions, both monotonic and cyclic.

The results obtained in the present study clearly demonstrate the importance of plastic strain rate on the damage-accumulation processes. Thus, for example, in a low-cycle fatigue test with tensile hold time only, the damage accumulated during the hold time will be greater for a cyclic relaxation test than for a cyclic creep test with the same creep strain increment during the hold time. This is contrary to one of the basic postulates of the strain-range partitioning technique where the damage in cyclic creep is assumed to be identical to the damage in cyclic relaxation provided the accumulated creep strains are equal. The strain-range partitioning technique implicitly assumes that predictions for cyclic-relaxation tests with long hold times can be made by obtaining data from cyclic creep tests which can be run in the laboratory in much shorter times. The present analysis suggests that such a procedure can be highly unconservative, particularly for cyclic-relaxation tests at small strain ranges with long hold times which are of great interest to designers. To demonstrate this, first consider a cyclic creep test with creep strain $\Delta\varepsilon_{cp}$ accumulated during the hold time of each cycle. Manson et al.[8] had originally proposed a linear damage rule according to which the damage during the hold time, denoted by $1/N_{cp}$, was related to $\Delta\varepsilon_{cp}$ by a power law and was determined by best fit from test data. The damage can be calculated by the present method by integrating Eq. (1) over the hold-time period as

$$\frac{1}{N_{cp}} = T \left(\frac{\Delta\varepsilon_p}{2}\right)^m \int_0^{t_H} \dot{\varepsilon}_p^{\ k} \, dt$$

or

$$\frac{1}{N_{cp}} = T \left(\frac{\Delta\varepsilon_p}{2}\right)^m \dot{\varepsilon}_p^{\ k} \, t_H \, .$$

Noting that $\dot{\varepsilon}_p \, t_H \approx \Delta\varepsilon_{cp}$, the above reduces to

$$\frac{1}{N_{cp}} = T \left(\frac{\Delta\varepsilon_p}{2}\right)^m \dot{\varepsilon}_p^{\ k-1} \, \Delta\varepsilon_{cp} \tag{11}$$

or

$$N_{cp} = \frac{1}{T} \left(\frac{\Delta\varepsilon_p}{2}\right)^{-m} \dot{\varepsilon}_p^{\ 1-k} \, \Delta\varepsilon_{cp}^{\ -1} \, . \tag{12}$$

Using the values $T = 0.64$, $m = 0.92$, and $k = 0.525$ for Type 304 stainless steel at 593°C from Fig. 1 and approximately relating $\dot{\varepsilon}_p$ to the plastic strain range $\Delta\varepsilon_p$ (from the last two tests in Table I) by

$$\dot{\varepsilon}_p = 2.75 \times 10^{-6} \left(\frac{\Delta\varepsilon_p}{2}\right)^{0.44} ,$$

Eq. (12) can be reduced to

$$N_{cp} = 3.57 \times 10^{-3} \left(\frac{\Delta\varepsilon_p}{2}\right)^{-0.71} \Delta\varepsilon_{cp}^{\ -1} \, . \tag{13}$$

Equation (13) shows that N_{cp} is not uniquely related to $\Delta\varepsilon_{cp}$ because it also depends on the plastic strain range.

Subsequently, to obtain a better prediction of fatigue life, Manson[9] proposed the interaction damage rule that stated the damage during the hold time is given by $(\Delta\varepsilon_{cp}/\Delta\varepsilon_p)/N_{cp}$. Replacing the left-hand side of Eq. (11) by $(\Delta\varepsilon_{cp}/\Delta\varepsilon_p)/N_{cp}$ and proceeding as before, the following can be derived:

$$N_{cp} = 1.784 \times 10^{-3} \left(\frac{\Delta\varepsilon_p}{2}\right)^{-1.71} \, . \tag{14}$$

Thus, the interaction damage rule provides a power-law relationship between N_{cp} and $\Delta\varepsilon_p$, independent of $\Delta\varepsilon_{cp}$, for the cyclic creep tests. Equations (12) and (14) also explain why the interaction damage rule was favored over the linear damage rule. A plot of Eq. (14) is shown in Fig. 16, and it is close to the N_{cp} versus $\Delta\varepsilon_p$ plot reported by Diercks[10] who obtained the plot directly from cyclic creep data. However, the relationship between N_{cp} and $\Delta\varepsilon_p$ for cyclic-relaxation tests is not as simple as Eq. (14) because it involves $\Delta\varepsilon_{cp}$. This is due to the fact that, unlike the cyclic creep tests, the plastic strain rate during the hold-time period of cyclic-relaxation tests decreases continuously with time. Values of N_{cp}, for the cyclic-relaxation tests given in Table I, can be calculated by equating the hold-time damage reported in Table I with $(\Delta\varepsilon_{cp}/\Delta\varepsilon_p)/N_{cp}$. Eight such values are shown in Fig. 16, which also includes the duration of hold time in minutes per cycle of each test. Note that the N_{cp} values computed from the cyclic-relaxation tests are smaller than those computed from the cyclic creep tests, and the difference is larger the larger the hold time and smaller the plastic strain range. Thus, the use of the N_{cp} versus $\Delta\varepsilon_p$ curve obtained from cyclic creep tests carried out at large strain ranges to calculate lives of specimens subjected to cyclic relaxation at small strain ranges with long hold times by the strain-range partitioning method could result in highly unconservative estimates. It is interesting to note that Diercks.[10] in his analysis of Type 304 stainless steel fatigue data by the strain-range partitioning technique, observed that a better prediction for cyclic-relaxation tests could be made by a $\Delta\varepsilon_p$ versus N_{cp} curve, which lies to the left of the curve derived from cyclic creep data.

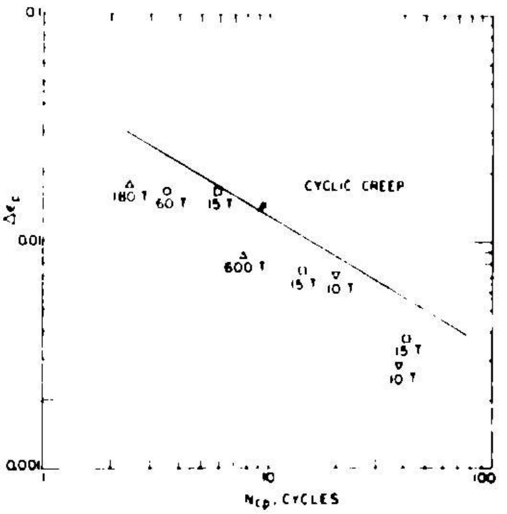

Fig. 16. Calculated $\Delta\varepsilon_p$ vs N_{cp} Values for Type 304 Stainless Steel at 593°C Using Cyclic Creep and Cyclic Relaxation Lives. Neg. No. MSD-61843.

Another topic that is of considerable interest to the designers in low-cycle fatigue is "saturation," i.e., whether the cycles to failure reach a lower limit for a sufficiently long hold-time period beyond which an additional increase in hold time does not affect the cyclic life. According to the present approach, saturation will occur only if the plastic strain rate becomes zero, i.e., no additional stress relaxation during the hold time. Figure 15 shows that the stress versus plastic strain-rate plot obtained from a stress-relaxation test tends to level off at a strain rate of 10^{-9} s^{-1}. However, insufficient data points exist at slower strain rates with which to establish that no additional stress relaxation occurs. A similar trend is also exhibited in the stress-relaxation plot of test 528 (Fig. 9) at a hold time of 600 min. If the slope of the stress-relaxation curve reaches zero or close to zero, then, according to the present analysis, saturation will occur for all practical purposes. This, however, cannot be concluded at the present time without performing additional tests that involve a longer hold time than 600 min. In addition, the hold time to saturation, if it occurs, will also depend on the strain range and temperature. Furthermore, the effects of aging and an active environment will become important in long hold-time tests. These effects cannot be fully evaluated by means of short-term tests in the laboratory.

To study the effects of various wave shapes, four hypothetical tests (at 593°C) with tensile hold times only were selected for Type 304 stainless steel. Each case was analyzed for a constant plastic strain range of 1.7% with tensile hold times ranging from 1 to 180 min. In all cases, an average time of 10 s was allowed for the cyclic part of each cycle. This cycle, referred to as the trapezoidal case, was, in turn, replaced by continuous triangular, parabolic, and sinusoidal wave forms (Appendix B, Fig. B.1) with the same strain range and time period as the trapezoidal case. The damage for the trapezoidal case was analyzed by using relaxation data obtained from ANL tests. The damage for the continuous cycling was calculated by using Eqs. (B.7)-(B.9), depending on whether the equivalent plastic strain rate corresponded to the intergranular, mixed mode, or transgranular failure mode. The results displayed in Table II show that replacement of a trapezoidal strain cycle by a triangular, parabolic, or sinusoidal wave shape does not influence the fatigue life significantly. The implication of the above exercise is that, in tensile hold-time tests, wave-shape effects are not significant, at least for the wave shapes and time periods considered. Because of the weak dependence of fatigue lives on wave-shape effects, Coffin's frequency-modified life equation can be extended to predict the influence of tensile hold times on fatigue life with some success.[33]

TABLE II. Effect of Wave Shapes on Low-cycle Fatigue Life of Type 304 Stainless Steel at 593°C

$\Delta\varepsilon_p$, %	τ, s	Predicted N_f Trapezoidal Case	$\dot{\varepsilon}_{p_{ave}}$, s^{-1}	Predicted N_f Triangular Case	Predicted N_f Parabolic Case	Predicted N_f Sinusoidal Case
1.7	70	440	4.79×10^{-4}	410	378	369
1.7	910	220	3.73×10^{-5}	184	191	183
1.7	3610	141	9.42×10^{-6}	118	123	118
1.7	10810	75	3.14×10^{-6}	57	59	57

However, the preceeding conclusions are not valid for cycles with compressive or symmetric hold time or for cycles with a highly asymmetric shape, such as in the case of sawtooth cycling (Fig. 17) where a cycle may consist of a slow rate of loading followed by a fast rate of unloading (slow-fast) or vice versa (fast-slow). Although these types of tests have not been performed at ANL, it may be shown by the present approach that, for Type 304 stainless steel, slow-fast cycling would be more damaging than fast-slow cycling. Coffin has experimentally observed such a behavior for Type 304 stainless steel.

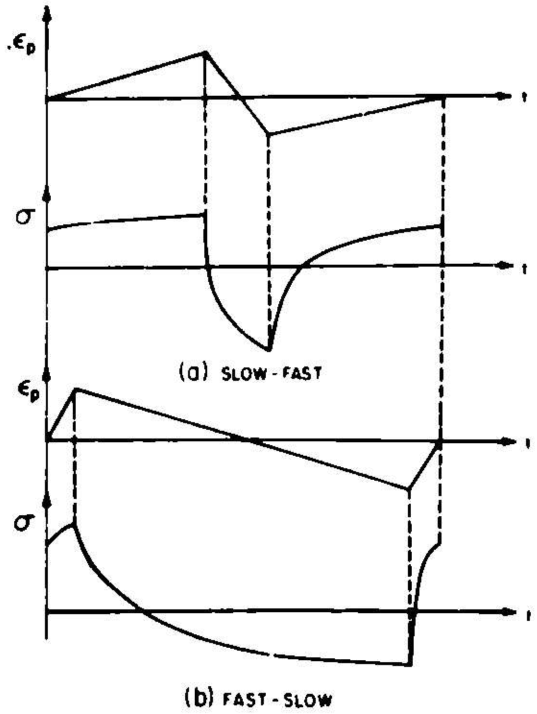

Fig. 17. Schematic of Variations of Stress and Plastic Strain with Time during Sawtooth Cycling. Neg. No. MSD-62311.

To show this, first note that, according the present analysis, the damage incurred during the high strain-rate portion of the cycle is small compared with that incurred during the slow strain-rate part of the cycle and may be ignored in the present discussion. Also, during a slow rate of straining, approximately four times more damage is accumulated in the presence of tensile stress than in the presence of compressive stress. Figure 17a shows that the majority of the time spent in the slow part of a slow-fast cycle is under tension, whereas Fig. 17b shows that the majority of the time spent in the slow part of a fast-slow cycle is under compression. Consequently, the slow-fast cycling would be more damaging than the fast-slow cycling, although a mean compressive stress is present in the former case and a mean tensile stress is present in the latter.

In addition to wave shape, other variables must be considered, such as surface roughness[34,35] and environmental effects.[36,37] It is important to note that the values of the material parameters used in calculating creep fatigue damage in the present report are based on fatigue test results obtained in air. These parameters may be different for different environments. In addition, these parameters will be functions of temperature -- a subject that is currently under investigation at ANL. Tests with different strain rates and hold times conducted under ultrahigh vacuum conditions ($<10^{-8}$ Torr) with known impurity levels in the environment chamber should clarify the role of the environment in creep-fatigue interaction. Such tests are currently in progress at ANL.

VIII. CONCLUSIONS

A creep fatigue-damage-rate equation in terms of current plastic strain, strain rate, and a characteristic crack length has been presented. Although the basic approach is phenomenological, it can be justified qualitatively from a mechanistic viewpoint. The method so far has been successfully applied to compute damage and analyze the failure behavior of Type 304 stainless steel at 593°C under various monotonic and cyclic loading conditions. Since the basic damage equation is of an incremental type, it has a potential use for analyzing damage due to several deformation paths that are of interest to designers of structural components which operate at elevated temperatures. Additional tests involving different materials and temperatures and more complicated loading histories are required to verify the present approach.

ACKNOWLEDGMENTS

The authors would like to express gratitude to Professor Che-Yu Li for valuable discussions on creep fatigue-damage mechanisms. Thanks are also due J. R. Lloyd for painstakingly reducing all the relaxation data and R. W. Weeks and D. R. Diercks for encouragement.

REFERENCES

1. *Interpretation of the ASME Boiler and Pressure Vessel Code, Case 1592*, American Society of Mechanical Engineers, New York, 1974.

2. S. S. Manson, "Interfaces between Fatigue, Creep, and Fracture," Intl. J. Fracture Mechanics 2(1), 327 (1966).

3. L. F. Coffin, "Predictive Parameters and Their Application to High Temperature, Low Cycle Fatigue," in *Fracture 1969* (Proc. Second Intl. Conf. on Fracture), Chapman and Hall, London, 1969, p. 643.

4. L. F. Coffin, "The Effect of Frequency on the Cyclic Strain and Low Cycle Fatigue Behavior of Cast Udimet 500 at Elevated Temperature," Met. Trans. 2, 3105 (1971).

5. J. B. Conway, J. T. Berling, and R. H. Stentz, *A New Correlation of the Effects of Hold Time on Low-cycle Fatigue Behavior*, General Electric Company, GEMP-702 (June 1969).

6. R. W. Weeks, D. R. Diercks, and C. F. Cheng, *ANL Low-cycle Fatigue Studies -- Program, Results, and Analysis*, Argonne National Laboratory, ANL-8009 (November 1973).

7. C. F. Cheng, C. Y. Cheng, D. R. Diercks, and R. W. Weeks, "Low-Cycle Fatigue Behavior of Types 304 and 316 Stainless Steel at LMFBR Operating Temperature," in *Fatigue at Elevated Temperatures*, American Society for Testing and Materials, Philadelphia, 1973, ASTM STP-520, pp. 355-364.

8. S. S. Manson, G. R. Halford, and M. H. Hirschberg, "Creep-Fatigue Analysis by Strain-Range Partitioning," in *Design for Elevated Temperature Environment*, American Society of Mechanical Engineers, New York, 1971, pp. 12-28.

9. S. S. Manson, "The Challenge to Unify Treatment of High Temperature Fatigue -- A Partisan Proposal Based on Strain-Range Partitioning," in *Fatigue at Elevated Temperatures*, American Society for Testing and Materials, Philadelphia, 1973, ASTM STP-520, pp. 744-782.

10. D. R. Diercks, "The Application of Strainrange Partitioning to the Prediction of Elevated-temperature, Low-cycle Fatigue Life for Type 304 Stainless Steel," in *Advances in Design for Elevated Temperature Environment*, American Society of Mechanical Engineers, New York, 1975, pp. 29-38.

11. E. L. Robinson, "Effect of Temperature Variation on the Long-time Rupture Strength of Steels," Trans. ASME 74(5), 777 (1952).

12. D. A. Spera, *Calculation of Thermal-fatigue Life Based on Accumulated Creep Damage*, NASA Technical Note, NASA-TN-D-5489 (1969).

13. P. S. Maiya, "Considerations of Low Crack Initiation and Crack Propagation in Low-Cycle Fatigue," Scripta Met. 9(11), 1141-1146 (1975).

14. E. W. Hart, "A Phenomenological Theory for Plastic Deformation of Polycrystalline Metals," Acta Met. 18, 599 (1970).

15. F. Garofalo, *Fundamentals of Creep and Creep-Rupture in Metals*, The MacMillan Company, New York, 1965.

16. J. B. Conway, R. H. Stentz, and J. T. Berling, *Fatigue, Tensile, and Relaxation Behavior of Stainless St· ·ls*, TID-26135, prepared for Division of Reactor Research and Development, published by Technical Information Center, Office of Information Services, U. S. Atomic Energy Commission (1975).

17. D. R. Diercks and W. F. Burke, "Elevated-Temperature True Stress— True Strain Tensile Behavior of AISI Type 304 Stainless Steel," in *Elevated Temperature Properties of Austenitic Stainless Steels*, American Society of Mechanical Engineers, New York, 1974, pp. 19-30.

18. F. C. Monkman and N. J. Grant, "An Empirical Relationship Between Rupture Life and Minimum Creep Rate," in Proc. ASTM 56, 593 (1956).

19. *Mechanical Properties Test Data for Structural Materials Quarterly Progress Report for Period ending October 31, 1974*, Oak Ridge National Laboratory, ORNL-5103, pp. 109-118.

20. *Mechanical Properties Test Data for Structural Materials Quarterly Progress Report for Period ending April 30, 1974*, Oak Ridge National Laboratory, ORNL-4963, pp. 61-81.

21. *Mechanical Properties Test Data for Structural Materials Quarterly Progress Report for Period ending January 31, 1974*, Oak Ridge National Laboratory, ORNL-4948, pp. 17?-187.

22. R. W. Swindeman, Oak Ridge National Laboratory, private communication (1975).

23. M. Gell and G. R. Leverant, "Mechanisms of High-Temperature Fatigue," in *Fatigue at Elevated Temperatures*, American Society for Testing and Materials, Philadelphia, 1973, ASTM STP-520, pp. 37-66.

24. R. L. Bell and T. G. Langdon, "Grain-boundary Sliding," in *Interfaces Conference*, R. C. Gifkins, ed., Butterworths, London, 1969, pp. 115-137.

25. J. Mancuso, F. Huang, and Che-Yu Li, "Growth of Grain Boundary Cavities under Applied Stress and Irradiation," presented at *Intl. Conf. on Fundamental Aspects of Radiation Damage in Metals*, Gatlinburg, Tennessee, October 5-10, 1975.

26. H. E. Evans, "The Mechanism of Void Growth and Factors Affecting the Onset of Intergranular Failure During Creep of a Mg-08% Al Alloy," Metal Sci. J. 3, 33-38 (1969).

27. H. E. Evans and R. P. Skelton, "Grain-boundary Sliding and Cavity Growth During the High-temperature Fatigue of Magnox A180," Metal Sci. J. 3, 152-155 (1969).

28. A. Gittus, "The Mechanisms of Cavity Growth in Copper During High Temperature Fatigue," Metal Sci. J. 2, 51-58 (1968).

29. G. J. Hill, "The Failure of Wrought 1% Cr-Mo-V Steels in Reversed Bending High-strain Fatigue at 550°C," in *Thermal and High-strain Fatigue*, The Metals and Metallurgy Trust of the Institute of Metals and the Institute of Metallurgists, London, Monograph and Report Series No. 32, pp. 312-327 (1967).

30. E. W. Hart, C. Y. Li, H. Yamada, and G. L. Wire, "Phenomenological Theory: A Guide to Constitutive Relations and Fundamental Deformation Properties," in *Constitutive Equations in Plasticity*, Ali S. Argon, ed., MIT Press, Cambridge, 1975, pp. 149-197.

31. Che-Yu Li, *Grain Boundary Sliding and Structure*, AEC Progress Report COO-2172-7, 1973-74, Cornell University.

32. Che-Yu Li, *Grain Boundary Sliding and Structure*, AEC Progress Report COO-2172-11, 1974, Cornell University.

33. P. S. Maiya and S. Majumdar, *Application of Frequency-modified Life Approach to the Low-cycle Fatigue Behavior of Type 304 Stainless Steel*, Argonne National Laboratory, ANL-76-40 (May 1976).

34. P. S. Maiya and D. E. Busch, "Effect of Surface Roughness on Low-Cycle Fatigue Behavior of Type 304 Stainless Steel," Met. Trans. A 6A(9), 1761-1766 (1975).

35. P. S. Maiya, "Effects of Surface Roughness and Strain Range on the Low-Cycle Fatigue Behavior of Type 304 Stainless Steel," Scripta Met. 9, 1277 (1975).

36. L. F. Coffin, "The Effect of High Vacuum on the Low Cycle Fatigue Law," Met. Trans. 3, 1777 (1972).

37. D. A. Woodford and L. F. Coffin, "The Role of Grain Boundaries in High Temperature Fatigue," in *Grain Boundaries in Engineering Materials*, J. L. Walter, J. H. Westbrook, and D. A. Woodford, eds., Claitor's Publishing Division, Baton Rouge, Louisiana, 1975, p. 421.

Addendum

H. D. Solomon, Met. Trans. 4, 341-347 (1973).

After the present report was completed, the authors were informed of the publication by Solomon in which he proposed an equation similar to our Eq. (1). However, he used frequency instead of plastic strain rate to study macroscopic crack propagation.

APPENDIX A

Damage Due to Continuous Cycling at Constant Plastic Strain Rate

Figure A.1 contains the typical stress response for a constant plastic strain-rate fatigue test with strain range $\Delta\varepsilon_p$ and time period τ. Note that the stress and plastic strain do not simultaneously achieve zero values. Assuming the hysteresis loop shape is symmetric, the damage during the tension half of the cycle, D_T, is obtained from integrating Eq. (1) as

$$D_T = D_{ab} + D_{bc} + D_{cd} = T \int_0^{\tau/2} |\varepsilon_p|^m \, |\dot{\varepsilon}_p|^k \, dt$$

$$D_{ab} = T \int_0^{\tau_1} |\dot{\varepsilon}_p t - \dot{\varepsilon}_p \tau_1|^m \, |\dot{\varepsilon}_p|^k \, dt$$

$$= T \int_0^{\tau_1} \left[\dot{\varepsilon}_p (\tau_1 - t)\right]^m |\dot{\varepsilon}_p|^k \, dt$$

$$= T \int_0^{\tau_1} |\dot{\varepsilon}_p t|^m \, |\dot{\varepsilon}_p|^k \, dt \qquad \text{(A.1)}$$

$$D_{bc} = T \int_{\tau_1}^{\tau_1+\tau/4} |\dot{\varepsilon}_p t - \dot{\varepsilon}_p \tau_1|^m \, |\dot{\varepsilon}_p|^k \, dt$$

$$= T \int_{\tau_1}^{\tau_1+\tau/4} \left[\dot{\varepsilon}_p (t - \tau_1)\right]^m |\dot{\varepsilon}_p|^k \, dt$$

$$= T \int_0^{\tau/4} |\dot{\varepsilon}_p t|^m \, |\dot{\varepsilon}_p|^k \, dt \qquad \text{(A.2)}$$

$$D_{cd} = T \int_{\tau_1+\tau/4}^{\tau/2} \left| \left[\frac{\Delta\varepsilon_p}{2} - \dot{\varepsilon}_p (t - \tau_1 - \tau/4)\right] \right|^m |\dot{\varepsilon}_p|^k \, dt \,.$$

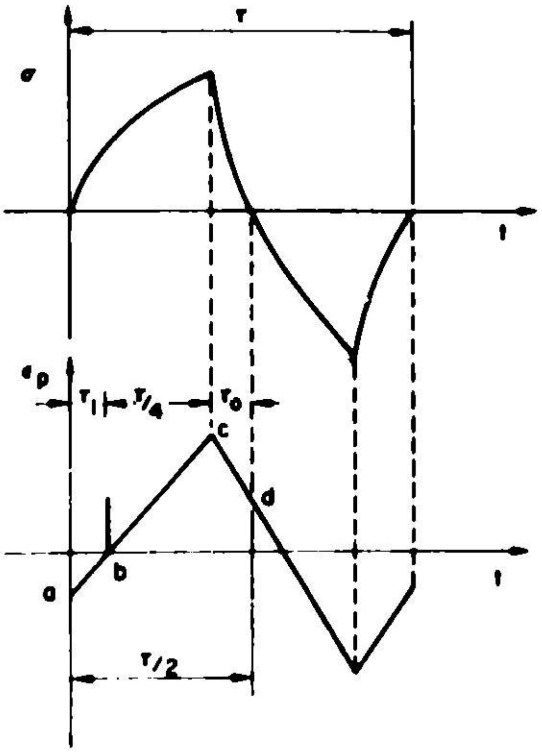

Fig. A.1. Schematic of Variations of Stress and Strain with Time during Continuous Cycling. Neg. No. MSD-61839.

Noting that $\Delta\epsilon_p/2 = \tau\dot{\epsilon}_p/4$, then

$$D_{cd} = T \int_{\tau_1+\tau/4}^{\tau/2} \left|\dot{\epsilon}_p\left[\frac{\tau}{2} - t + \tau_1\right]\right|^m |\dot{\epsilon}_p|^k \, dt$$

$$= T \int_{\tau_1}^{\tau/4} |\dot{\epsilon}_p t|^m |\dot{\epsilon}_p|^k \, dt \, . \qquad \text{(A.3)}$$

Adding Eqs. (A.1)-(A.3),

$$D_T = 2T \int_o^{\tau/4} |\dot{\epsilon}_p t|^m |\dot{\epsilon}_p|^k \, dt \, .$$

Similarly, the damage for the compression half of the cycle, D_c, is given by

$$D_c = 2C \int_o^{\tau/4} |\dot{\epsilon}_p t|^m |\dot{\epsilon}_p|^k \, dt \, .$$

Thus, the total damage per cycle is

$$D_T + D_c = 2(T + C) \int_o^{\tau/4} |\dot{\epsilon}_p t|^m |\dot{\epsilon}_p|^k \, dt \, . \qquad \text{(A.4)}$$

APPENDIX B

Wave-shape Effects

Consider three types of strain cycling, each with the same plastic strain range $\Delta\epsilon_p$ and time period τ but one with constant plastic strain rate so that (Fig. B.1)

$$\epsilon_p(t) = \frac{\Delta\epsilon_p}{2}\left(\frac{4t}{\tau} - 1\right), \quad o \le t \le \tau/2. \tag{B.1}$$

A second follows a parabolic law so that

$$\epsilon_p(t) = \frac{\Delta\epsilon_p}{2}\left(\frac{8t^2}{\tau^2} - 1\right), \quad o \le t \le \tau/2, \tag{B.2}$$

and the third follows a sinusoidal form so that

$$\epsilon_p(t) = -\frac{\Delta\epsilon_p}{2}\cos(2\pi\, t/\tau)\ . \tag{B.3}$$

The cycles to failure for the first case is given by Eq. (2) as

$$N_{f_1} = \frac{m+1}{4A}\left(\frac{\Delta\epsilon_p}{2}\right)^{-(m+1)}\left(\frac{2\Delta\epsilon_p}{\tau}\right)^{1-k}$$

or

$$N_{f_1} = \frac{m+1}{4A}\left(\frac{\Delta\epsilon_p}{2}\right)^{-(m+k)}\left(\frac{4}{\tau}\right)^{1-k}\ . \tag{B.4}$$

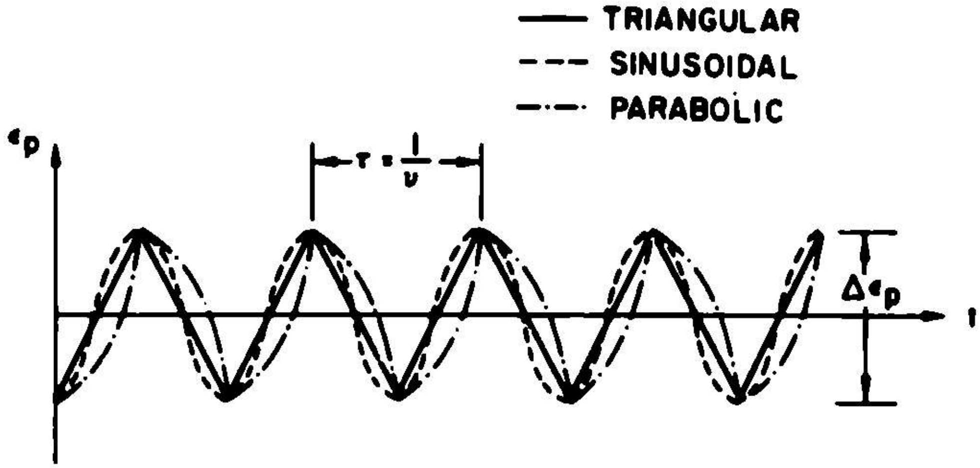

Fig. B.1. Schematic of Various Wave Shapes.
Neg. No. MSD-61788.

Parabolic Case

For the second case integrating Eq. (1) and using Eq. (B.2),

$$\ln \frac{a_c}{a_o} = N_{f_2} \left[(T + C) \int_o^{\tau/2} \left(\frac{8\Delta\epsilon_p t}{\tau^2} \right)^k \left| \frac{4\Delta\epsilon_p t^2}{\tau^2} - \frac{\Delta\epsilon_p}{2} \right|^m dt \right] .$$

Using Eq. (2a),

$$\frac{1}{N_{f_2}} = 2A \left(\frac{\Delta\epsilon_p}{2} \right)^{m+k} (\tau)^{1-k} \frac{1}{\tau} \int_o^{\tau/2} \left(\frac{16t}{\tau} \right)^k \left| \frac{8t^2}{\tau^2} - 1 \right|^m dt .$$

Since m is close to unity in all cases (Fig. 1), the integral above is evaluated approximately by putting $m = 1$ to give

$$\frac{1}{N_{f_2}} = 2^{k+2} \left[\frac{2}{k+1} \left(\frac{1}{\sqrt{2}} \right)^{k+1} - \frac{1}{k+1} + \frac{2}{k+3} - \frac{4}{k+3} \left(\frac{1}{\sqrt{2}} \right)^{k+3} \right] \times$$

$$A \left(\frac{\Delta\epsilon_p}{2} \right)^{m+k} \left(\frac{\tau}{4} \right)^{1-k} . \qquad \text{(B.5)}$$

Sinusoidal Case

For the third case integrating Eq. (1) and using Eq. (B.3),

$$\ln \frac{a_c}{a_o} = N_{f_3} \left[2(T + C) \int_o^{\tau/4} \left(\frac{\Delta\epsilon_p}{2} \right)^{k+m} (\cos 2\pi t/\tau)^m \left(\frac{2\pi}{\tau} \sin 2\pi t/\tau \right)^k dt \right]$$

or, using Eq. (2a),

$$\frac{1}{N_{f_3}} = 4A \left(\frac{\Delta\epsilon_p}{2} \right)^{k+m} \left(\frac{2\pi}{\tau} \right)^k \int_o^{\tau/4} \left(\cos \frac{2\pi t}{\tau} \right)^m \left(\sin \frac{2\pi t}{\tau} \right)^k dt .$$

Making the approximation $m = 1$, the above can be reduced to

$$\frac{1}{N_{f_3}} = \frac{4A}{k+1} \left(\frac{\Delta\epsilon_p}{2} \right)^{k+m} (\tau/2\pi)^{1-k} . \qquad \text{(B.6)}$$

"Intergranular" Case

In the "intergranular" case ($\dot{\varepsilon}_p < 10^{-6}\ s^{-1}$), A = 0.4, k = 0.525, and m = 0.92. Putting these values in Eqs. (B.4)-(B.6),

$$N_{f_1} = 2.318 \left(\frac{\Delta\varepsilon_p}{2}\right)^{-1.445} (1/\tau)^{0.475}$$

$$N_{f_2} = 2.396 \left(\frac{\Delta\varepsilon_p}{2}\right)^{-1.445} (1/\tau)^{0.475}$$

$$N_{f_3} = 2.282 \left(\frac{\Delta\varepsilon_p}{2}\right)^{-1.445} (1/\tau)^{0.475} . \quad \text{(B.7)}$$

"Mixed-mode" Case

In the "mixed-mode" case ($10^{-6}\ s^{-1} < \dot{\varepsilon}_p < 10^{-4}\ s^{-1}$), A = 0.45, k = 0.62, and m = 0.93. Putting these values in Eqs. (B.4)-(B.6),

$$N_{f_1} = 1.834 \left(\frac{\Delta\varepsilon_p}{2}\right)^{-1.55} (1/\tau)^{0.38}$$

$$N_{f_2} = 1.907 \left(\frac{\Delta\varepsilon_p}{2}\right)^{-1.55} (1/\tau)^{0.38}$$

$$N_{f_3} = 1.828 \left(\frac{\Delta\varepsilon_p}{2}\right)^{-1.55} (1/\tau)^{0.38} . \quad \text{(B.8)}$$

"Transgranular" Case

In the "transgranular" case ($\dot{\varepsilon}_p > 10^{-4}\ s^{-1}$), A = 11.84, k = 0.81, and m = 1.19. Putting these values in Eqs. (B.4)-(B.6),

$$N_{f_1} = 0.0605 \left(\frac{\Delta\varepsilon_p}{2}\right)^{-2} (1/\tau)^{0.19}$$

$$N_{f_2} = 0.0558 \left(\frac{\Delta\varepsilon_p}{2}\right)^{-2} (1/\tau)^{0.19}$$

$$N_{f_3} = 0.0544 \left(\frac{\Delta\varepsilon_p}{2}\right)^{-2} (1/\tau)^{0.19} . \quad \text{(B.9)}$$

APPENDIX C

Rising Mean Strain-rate Tests

Consider a constant rising mean strain rate ($\dot{\varepsilon}_m$) superimposed on cycles with constant plastic strain range $\Delta\varepsilon_p$ at a plastic strain rate $\dot{\varepsilon}_p$ ($\dot{\varepsilon}_p >> \dot{\varepsilon}_m$) such that after N cycles the mean strain is $N\,\dot{\varepsilon}_m\,(2\Delta\varepsilon_p)/\dot{\varepsilon}_p$ (Fig. C.1).

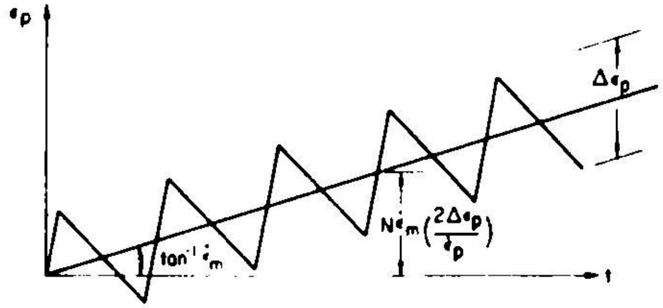

Fig. C.1. Plastic Strain vs Time Plot for a Typical Rising Mean Strain Rate Test. Neg. No. MSD-61790.

The crack growth per cycle after N cycles is then given by integrating Eq. (1) over one cycle [time period $\tau = (2\Delta\varepsilon_p)/\dot{\varepsilon}_p$] as

$$\frac{d\ln a}{dN} = (T + C)\int_{-\tau/4}^{\tau/4} \left|\frac{2N\Delta\varepsilon_p\dot{\varepsilon}_m}{\dot{\varepsilon}_p} + \dot{\varepsilon}_p t\right|^m |\dot{\varepsilon}_p|^k\,dt\,.$$

Defining

$$\alpha = \frac{4\dot{\varepsilon}_m}{\dot{\varepsilon}_p}\,,$$

the above can be reduced to

$$\frac{d\ln a}{dN} = (T + C)\,|\dot{\varepsilon}_p|^{k+m}\int_{-\tau/4}^{\tau/4}\left|\frac{\alpha N\tau}{4} + t\right|^m dt\,.$$

Taking into account that the integrand within the absolute sign changes sign at $N = 1/\alpha$, the above integral can be evaluated as

$$\frac{(m + 1)}{(T + C)}\left(\frac{\Delta\varepsilon_p}{2}\right)^{-(m+1)}|\dot{\varepsilon}_p|^{1-k}\,\frac{d\ln a}{dN} = \begin{cases}(1 - \alpha N)^{m+1} + (1 + \alpha N)^{m+1} & \text{for } N < \dfrac{1}{\alpha}\\[2ex] (\alpha N + 1)^{m+1} - (\alpha N - 1)^{m+1} & \text{for } N > \dfrac{1}{\alpha}\,.\end{cases}$$

Integrating the above equation from $a = a_o$ to $a = a_c$ and $N = 0$ to $N = N_f$ and transposing,

$$2\alpha(m+2)N_{f_o} = \begin{cases} (1+\alpha N_f)^{m+2} - (1-\alpha N_f)^{m+2} & \text{for } N_f < \frac{1}{\alpha} \\ (\alpha N_f + 1)^{m+2} - (\alpha N_f - 1)^{m+2} & \text{for } N_f > \frac{1}{\alpha}, \end{cases} \qquad (C.1)$$

where

$$N_{f_o} = \frac{m+1}{2(T+C)} \ln \frac{a_c}{a_o} \left(\frac{\Delta\varepsilon_p}{2}\right)^{-(m+1)} |\dot{\varepsilon}_p|^{1-k} .$$

Using Eq. (2a), the above equation can be rewritten as

$$N_{f_o} = \frac{m+1}{4A} \left(\frac{\Delta\varepsilon_p}{2}\right)^{-(m+1)} |\dot{\varepsilon}_p|^{1-k} .$$

Since m is close to unity in all cases (Fig. 1), the assumption of $m = 1$ enables one to simplify Eq. (C.1) to

$$N_f = \frac{1}{\alpha}\sqrt{\alpha N_{f_o} - \frac{1}{3}} \qquad \text{for } N_f > \frac{1}{\alpha}$$

and

$$\alpha^2 N_f^3 + 3N_f - 3N_{f_o} = 0 \qquad \text{for } N_f < \frac{1}{\alpha} . \qquad (C.2)$$